Acta Pharmaceutica Sinica B 2026;16(2):948−965

Chinese Pharmaceutical Association
Institute of Materia Medica, Chinese Academy of Medical Sciences

Acta Pharmaceutica Sinica B

www.elsevier.com/locate/apsb
www.sciencedirect.com

ORIGINAL ARTICLE

REEP6 promotes colorectal cancer glycolysis and tumorigenesis through PRMT5-mediated PGAM1 arginine methylation

Tuo Wang[a,b,c,†], Dongsheng Zhang[a,b,c,†], Chi Jin[a,b,c,†], Hengjie Xu[a,b,c,†], Hongxu Nie[a,b,c], Ye Wang[a,b,c], Chuan Zhang[a,b,c], Yifei Feng[a,b,c,*], Junwei Tang[a,b,c,*], Yueming Sun[a,b,c,d,*]

[a]*Department of General Surgery, Colorectal Institute of Nanjing Medical University, The First Affiliated Hospital of Nanjing Medical University, Nanjing 210029, China*
[b]*Jiangsu Province Engineering Research Center of Colorectal Cancer Precision Medicine and Translational Medicine, Nanjing 210029, China*
[c]*Collaborative Innovation Center for Cancer Personalized Medicine, Nanjing Medical University, Nanjing 210029, China*
[d]*The Affiliated Shuyang Hospital of Xuzhou Medical University, Suqian 223800, China*

Received 13 March 2025; received in revised form 7 June 2025; accepted 1 July 2025

KEY WORDS

Colorectal cancer;
REEP6;
Aerobic glycolysis;
PRMT5;
PGAM1;
Symmetric dimethylarginine;
Tumorigenesis;
Metabolic reprogramming

Abstract Metabolic reprogramming is a notable hallmark of cancer biology, especially aerobic glycolysis. Some clinical trials attempt to target cancer metabolism to develop therapeutic agents. However, the results have been not satisfactory. Here, we report that REEP6 is significantly upregulated and promotes glycolysis and tumorigenesis in CRC. Moreover, REEP6, as a molecular scaffolder, bridges the PRMT5−PGAM1 complex, which enhances the PRMT5-mediated symmetric dimethylarginine (SDMA) of PGAM1 at R40. The methylated PGAM1 possesses dramatically enhanced enzymatic activity and therefore boosts glycolytic flux in CRC cells. More than that, our results showed that combined treatment with specific shRNA and inhibitors exhibits synergistic anti-tumor efficacy in CRC, which may shed light on the development of a promising therapy in CRC.

*Corresponding authors.
E-mail addresses: fengyifei1982@163.com (Yifei Feng), pepsitjw@njmu.edu.cn (Junwei Tang), sunyueming@njmu.edu.cn (Yueming Sun).
[†]These authors made equal contributions to this work.
Peer review under the responsibility of Chinese Pharmaceutical Association and Institute of Materia Medica, Chinese Academy of Medical Sciences.

https://doi.org/10.1016/j.apsb.2025.10.025

1. Introduction

Colorectal cancer (CRC) ranks third in incidence and second in mortality globally, making it the most frequent digestive tract malignancy worldwide[1]. According to Global Cancer Statistics 2022, more than 1.9 million new cases and 904,000 deaths were estimated to occur in 2022[2]. Metabolic reprogramming has been widely recognized as an emerging biological hallmark of cancer, including CRC[3]. Numerous studies have been dedicated to developing such cancer therapeutic agents that could target cancer metabolism, and some were advancing to clinical trials[4-6]. However, clinical trials that target tumor metabolism for cancer therapy have sometimes shown unsatisfactory efficacy[6]. For this purpose, it is urgent to illustrate the exact molecular mechanisms that drive CRC metabolic reprogramming and therefore promote CRC tumorigenesis.

Protein arginine methyltransferases (PRMTs) are responsible for catalyzing the transfer of methyl group from *S*-adenosylmethionine (SAM) to the guanidine nitrogen atoms of specific arginine residues in target proteins, which results in the formation of three types of methylated arginine residue: monomethylarginine (MMA), asymmetric dimethylarginine (ADMA), and symmetric dimethylarginine (SDMA)[7]. As a type II arginine methyltransferase, protein arginine methyltransferase 5 (PRMT5) catalyzes the synthesis of SDMA on protein substrates[8]. Recently, PRMT5 has been identified as an oncoprotein in CRC progression due to its PRMT activity that regulate enzymatic activity, subcellular localization, and protein stability of target proteins[9,10]. For example, Liu et al. reported that PRMT5 methylated SMAD4 at R361, inducing SMAD complex formation and nuclear import[9]. PRMT5 directly catalyzes the SDMA of ALKBH5 at the R316 residue, which promotes TRIM28-mediated ALKBH5 ubiquitination and degradation[10].

Aerobic glycolysis also termed the Warburg effect, means that even in a sufficient oxygen supply, cancer cells preferentially consume glucose *via* the glycolysis pathway rather than oxidative phosphorylation[11,12]. It has been reported that aerobic glycolysis could be fueled by the upregulation of many glycolytic enzymes and transporters in cancer cells[13,14]. Among these, phosphoglycerate mutase 1 (PGAM1), a pivotal metabolic enzyme in the glycolysis pathway, has been a research hotspot for a long time[15]. The interconversion between 3-phosphoglycerate (3-PG) and 2-phosphoglycerate (2-PG) in glycolysis is critically catalyzed by PGAM1[16]. The aberrantly upregulated protein expression or overactivated enzymatic activity of PGAM1 was observed in various human cancers, including hepatocellular carcinoma (HCC) and non-small-cell lung cancer (NSCLC)[17-20]. Increasing studies have confirmed that multiple post-translational modifications (PTMs) of PGAM1 play a critical role in regulating its enzymatic activity[21-23]. For example, Tyr26 phosphorylation of PGAM1 enhances and stabilizes H11 phosphorylation, and therefore activates PGAM1[21]. Histone acetyltransferase 1 (HAT1) succinylates PGAM1 at Lys99, increasing its enzymatic activity and promoting proliferation and tumorigenesis in many cancers[22]. William et al.[23] reported that under glucose restriction, NAD^+-dependent protein deacetylase Sirt1 deacetylates PGAM1 and then attenuates its catalytic efficiency. However, the identification and the function of other PTMs on PGAM1 remain largely elusive.

Receptor expression enhancing protein 6 (REEP6) belongs to the REEPs family, which was initially identified for its capacity to facilitate the plasma membrane expression of olfactory receptors, G protein-coupled receptors, and taste receptors[24]. Recent studies have revealed some novel roles of REEP6 in cancer cell biology[25-27]. A previous study reported that REEP5 and REEP6 interact with CXCR1 and then enhance IL8-stimulated endocytosis of CXCR1 which mediates cancer cell responses in lung cancer[25]. Xia and his colleagues[26] found that REEP6 suppressed ferroptosis in OSCC cells by maintaining endoplasmic reticulum homeostasis, contributing to OSCC progression. But even so, the role of REEP6 in cancer, especially in CRC, still requires further investigation.

In this report, we found that REEP6 is extremely upregulated in CRC tissues and promotes CRC tumorigenesis through enhancing glycolytic flux. Further analysis revealed that REEP6, acting as a molecular scaffold, consolidates the interaction between PRMT5 and PGAM1. Our results showed that the REEP6-PRMT5-PGAM1 heterotrimeric complex could enhance PRMT5-mediated SDMA modification of PGAM1 at the R40 residue, which dramatically increased PGAM1 enzymatic activity. More importantly, combined treatment with specific shRNA and inhibitors shows synergistic inhibitory efficacy in tumorigenesis and proliferation of CRC cell lines, PDO, and xenograft models. Taken together, our data support that targeting the REEP6−PRMT5−PGAM1 complex may be a promising therapeutic strategy for CRC.

2. Materials and methods

2.1. Human specimens and cell culture

All samples were collected from CRC patients with signed informed consent at our hospital. Formalin-fixed paraffin-embedded tissue microarrays (TMA) were constructed by Servicebio (Wuhan, China) including 48 cases of paired normal mucosa, CRC primary, and liver metastatic tumors, and 80 cases of CRC tissues and distal normal mucosa. The Ethics Committee of our hospital approved this study.

The cell lines DLD-1, RKO, and human embryonic kidney 293T (HEK-293T) were purchased from the Cell Bank of Type Culture Collection of the Chinese Academy of Sciences (Shanghai, China). All cells were cultured in the recommended medium (Gibco, USA) supplemented with 10% fetal bovine serum (FBS; Gibco, USA) and 1% penicillin/streptomycin (Gibco, USA).

2.2. Quantitative real-time PCR (qRT-PCR)

TRIzol reagent (Invitrogen, USA) was applied to extract the total RNA of cell lines and tissues according to the manufacturer's protocols. Total RNA was reversely transcribed to cDNA using HiScript RT Mix (Vazyme, Jiangsu, China). Then, the expression of mRNA was analyzed using the SYBR Premix Ex Taq Kit (TaKaRa Biotechnology, Dalian, China) with the Applied Biosystems 7500 Sequence Detection System using relative primers for amplification. The relative gene expression was determined by the StepOne platform (version 2.3), while the primer sequences

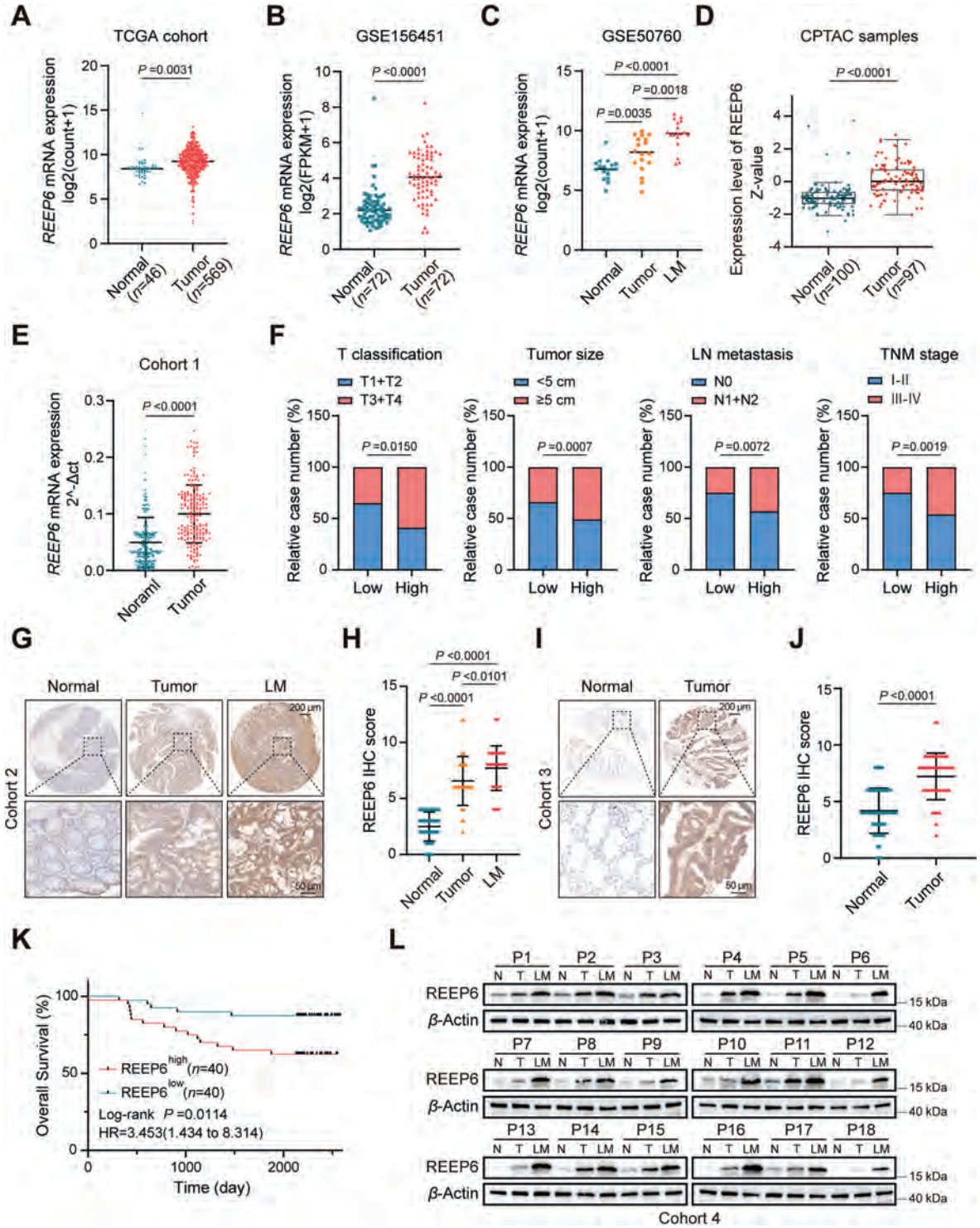

Figure 1 REEP6 is significantly overexpressed in CRC tissues. (A−C) The mRNA levels of REEP6 in the TCGA, GSE156451, and GSE50760 CRC cohorts. (D) The protein levels of REEP6 in the CPTAC CRC cohort. (E) The mRNA levels of REEP6 were measured by qRT-PCR in CRC tissues and matched adjacent normal tissues (cohort 1, $n = 200$). (F) Analysis of the correlation between REEP6 expression and clinicopathological factors in cohort 1. (G, H) Immunohistochemistry staining of REEP6 was performed in cohort 2 with 48 cases of CRC patients with liver metastasis. (G) Representative images of REEP6 expression (scale bars: 200 μm (upper), 50 μm (lower)), (H) Statistical analysis of IHC scores. (I−K) IHC analyses of REEP6 in cohort 3 with 80 cases of CRC patients. (I) Representative images of REEP6 expression (scale bars: 200 μm (upper), 50 μm (lower)), (J) the relative REEP6 expression was quantified by IHC scores, and (K) the Kaplan−Meier survival analysis of patients with $REEP6^{low}$ ($n = 40$) and $REEP6^{high}$ ($n = 40$) groups. (L) Immunoblotting analysis of REEP6 expression in cohort 4 with 18 cases of CRC patients with liver metastasis. All data are presented as the mean ± SD. *P*-values under 0.05 were considered statistically significant. *P* values were determined by the two-tailed Student's *t*-tests (A−E, H, and J), Chi-square test (F), and log-rank test (K).

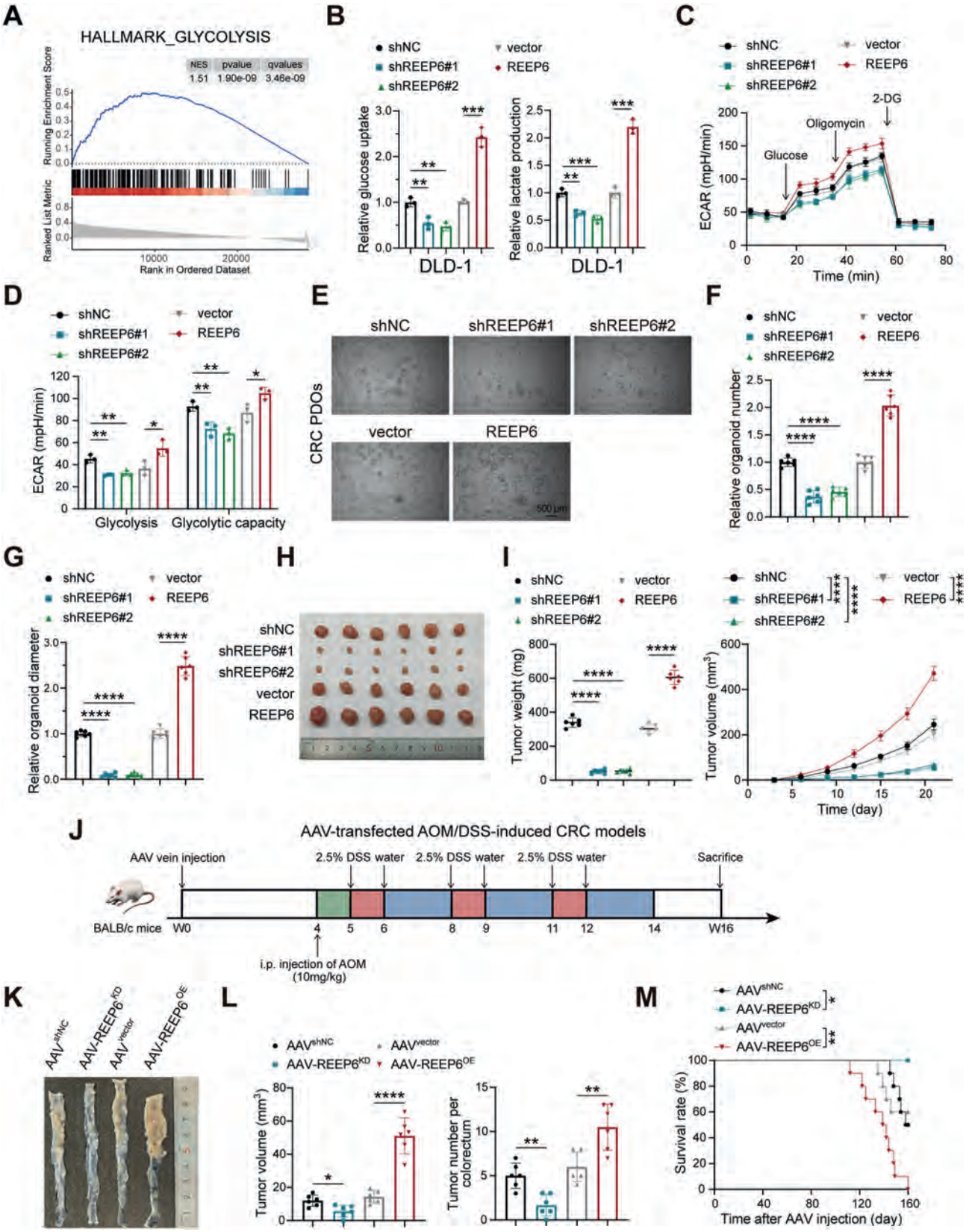

Figure 2 REEP6 facilitates glycolysis and tumorigenesis in CRC. (A) GSEA analysis of the TCGA database indicated that gene signatures representing the glycolysis pathways were enriched in patients with higher expression of REEP6 compared to those with lower expression of REEP6. (B) Glucose uptake and lactate production were detected in DLD-1 cells stably transfected *Lv*-sh*NC* and *Lv*-sh*REEP6* or *Lv-vecto*r and *Lv-REEP6* ($n = 3$). (C, D) Extracellular acidification rate (ECAR) was measured when REEP6 was stably overexpressed or knocked down in

for qRT-PCR can be referenced in Supporting Information Table S1.

2.3. Immunofluorescence (IF)

Cells were cultured in the confocal dish for 48 h and then washed with PBS three times. The cells were fixed with an immunostaining fixative overnight at 4 °C. Next, cells were blocked with blocking buffer and then incubated with primary antibody overnight at 4 °C. The cells were incubated with a secondary antibody for 60 min in the dark and then counterstained with 4′,6-diamidino-2-phenylindole (DAPI) as a nuclear indicator and imaged with a confocal laser-scanning microscope. The primary antibodies used are listed in Supporting Information Table S2.

2.4. Cell proliferation assays

The Cell Counting Kit-8 (Beyotime Biotechnology, Shanghai, China) and colony formation assays were performed as described previously[28].

2.5. Extracellular acidification rate (ECAR)

Seahorse XF Glycolysis Stress Test Kit (Agilent Technologies) was used for ECAR measurement by Seahorse Bioscience XF96 extracellular flux analyzer (Seahorse Bioscience). Briefly, CRC cells were seeded into the Seahorse plates and incubated overnight at 37 °C. The next day, the monolayer cells were washed with Seahorse buffer, and baseline concentration was measured. Then, glucose, oligomycin, and 2-deoxy-D-glucose were sequentially added for ECAR measurement. Data was analyzed by Seahorse XF96 Wave software.

2.6. Glucose uptake assay and lactate production assay

Quantification of glucose uptake and lactate production was performed with the Glucose Uptake Assay Kit (ab136955, Abcam) and L-Lactate Assay Kit (ab65331, Abcam), in accordance with the manufacturer's protocols as previously described[29].

2.7. 2-Phosphoglycerate (2-PG) and 3-phosphoglycerate (3-PG) assay

The measurement of 2-PG and 3-PG was conducted as previously described[30].

2.8. Animal models

The subcutaneous xenograft model was developed using 6-week-old male BALB/c nude mice. The mice were injected with 1×10^6 DLD-1 cells (stably transfected with the indicated lentiviruses) into the bilateral groin separately. Xenograft size was recorded at 3-day intervals, and the volume was derived from equation $L \times W^2/2$ (L: length, W: width). After 21 days, the animals were humanely euthanized to retrieve xenografts for statistical analysis. For combined treatment, the mice were intraperitoneally administered with PGMI-004A (MCE, 100 mg/kg) and/or GSK3326595 (MCE, 100 mg/kg) every 3 days. And the mice were euthanized on Day 30.

For the AOM/DSS-induced CRC model[31,32], four-week-old male BALB/c mice were injected into the tail veins with different AAVs as indicated. All mice were once administered azoxymethane (AOM, 10 mg/kg body weight, Sigma−Aldrich) intraperitoneally, then received 2.5% dextran sodium sulfate (DSS, MP) in drinking water for 7 days (1 week after azoxymethane injection), subsequently given normal water for 14 days. The DSS-normal water cycle was repeated in three rounds. Mice were euthanized at the end of the study to harvest their colon. All animal experiments were approved by the Committee on the Ethics of Animal Experiments of our university.

2.9. Statistical analysis

Statistical analyses were performed using GraphPad Prism 10.0 (GraphPad Software, San Diego, CA, USA) and IBM SPSS Statistics 26.0 (IBM Corp., Armonk, NY, USA). All experiments were independently repeated at least three times. Quantitative data are presented as mean ± standard deviation (SD). Statistical significance was determined using two-tailed Student's t-tests, Chi-square test, and Kaplan-Meier log-rank test. $P < 0.05$ was considered statistically significant.

3. Results

3.1. REEP6 is significantly overexpressed in CRC tissues

To elucidate the expression pattern of REEP6 in CRC tissues, we analyzed the mRNA level of REEP6 in The Cancer Genome Atlas (TCGA) and GEO (GSE156451 and GSE50760) databases. Compared to the normal tissues, REEP6 was significantly elevated in CRC tissues (Fig. 1A−C), moreover, CRC liver metastasis (CRLM) tissues had a more increased expression (Fig. 1C). Clinical Proteomic Tumor Analysis Consortium (CPTAC) datasets proved that REEP6 was highly expressed in colon cancer tissues than noncancerous tissues (Fig. 1D). The above result was further validated by our cohort 1 incorporating 200 cases of CRC patients (Fig. 1E). Statistical analyses of clinicopathological parameters in cohort 1 exhibited that REEP6 expression was positively correlated with T classification, tumor size, lymph node metastasis and TNM stage (Fig. 1F). Tissue microarray IHC staining of 48 CRLM patients in cohorts 2 and 80 cases of CRC patients (referred as cohorts 3) demonstrated that the protein levels of REEP6 were dramatically upregulated in

DLD-1 cells (C), and column statistics were shown in (D) ($n = 3$). (E−G) The representative images (E, scale bars: 500 μm) and the relative organoid number or diameter (F, G) in CRC patient-derived organoids (PDO) stably transfected with the indicated lentiviruses ($n = 6$). (H, I) Representative images (H) and statistical analyses (I) of the xenograft tumors in nude mice bearing DLD-1 cells stably transfected with the indicated lentiviruses. $n = 6$ mice per group. (J) schematic diagram of AAV-transfected AOM/DSS-induced CRC models in BALB/c mice. (K) The colorectums were opened longitudinally, and representative colorectal images were derived from AAV^{shNC}, $AAV\text{-}REEP6^{KD}$, and AAV^{vector}, $AAV\text{-}REEP6^{OE}$ mice from AOM/DSS-induced CRC models. (L) Tumor volumes and tumor numbers were calculated in each group. $n = 6$ mice per group. (M) Survival curves for the indicated mice. $n = 10$ mice per group. All data are presented as the mean ± SD. $^*P < 0.05$, $^{**}P < 0.01$, $^{***}P < 0.001$, $^{****}P < 0.0001$. P values were determined by the two-tailed Student's t-tests (B, D, F, G, I, and L), and Kaplan−Meier log-rank test (M). Lv, lentivirus; AAV, adeno-associated virus; AOM, azoxymethane; DSS, dextran sodium sulfate.

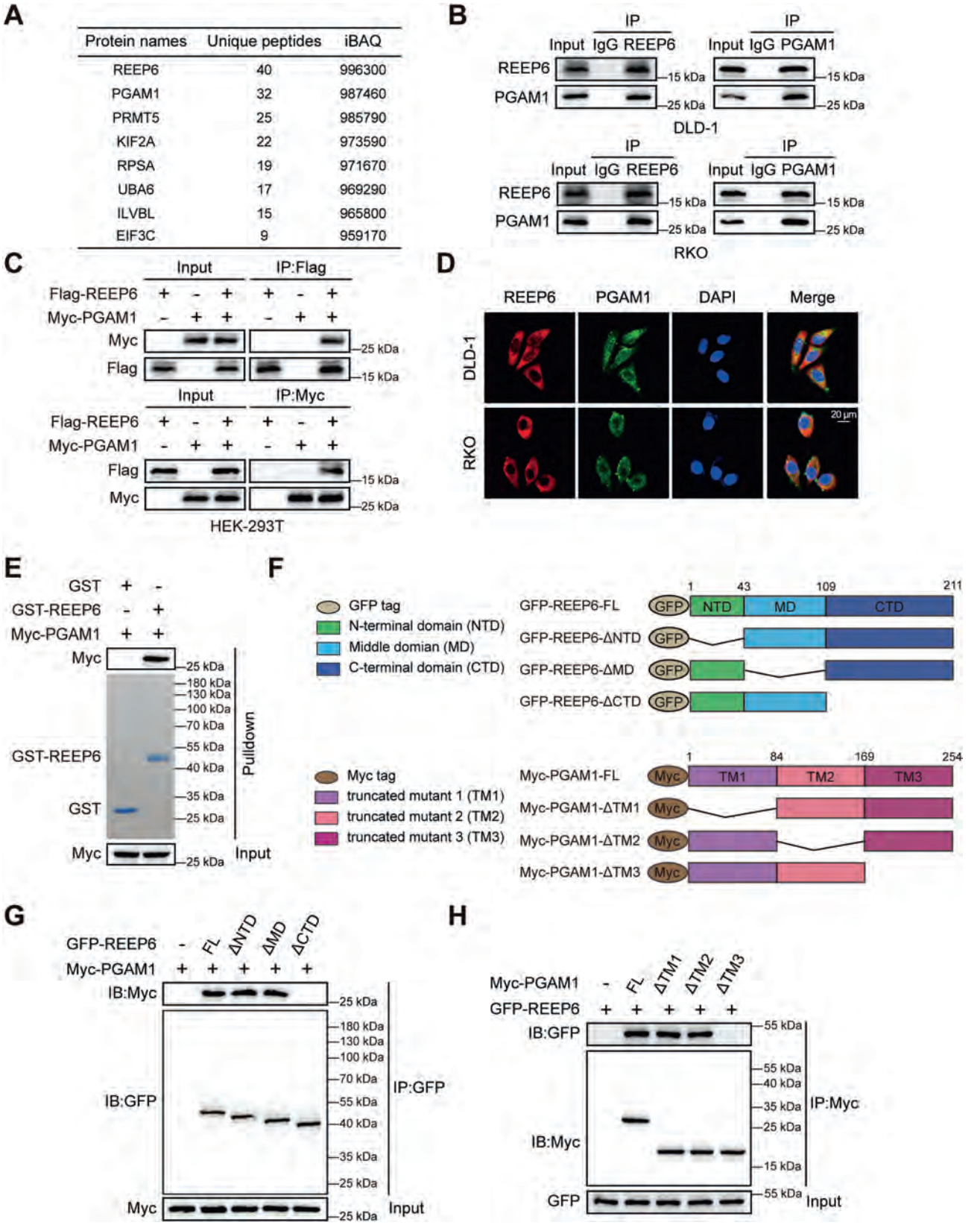

Figure 3 REEP6 interacts with PGAM1. (A) Candidates of REEP6-interacting proteins identified by immunoprecipitation (IP) and mass spectrometry analyses. (B) Reciprocal endogenous IP was performed to detect the interactions between PGAM1 and REEP6 in DLD-1 and RKO cells ($n = 3$). (C) The mutual interaction between ectopically expressed PGAM1 and REEP6 in HEK-293T cells. HEK-293T cells transfected with Flag-tagged REEP6 and Myc-tagged PGAM1, followed by IP with anti-Flag beads or anti-Myc beads and analyses by western blotting ($n = 3$). (D) Immunofluorescence (IF) analyses of endogenous PGAM1 and REEP6 in DLD-1 and RKO cells (scale bars: 20 μm). (E) The direct

CRLM and CRC tissues compared to adjacent normal tissues (Fig. 1G−J). Kaplan-Meier survival curve of cohort 3 showed that CRC patients with increased REEP6 expression had a worse overall survival (Fig. 1K). Furthermore, the analysis of the relation between REEP6 expression and clinicopathological factors in cohort 3 revealed that elevated REEP6 expression was positively associated with tumor size, T classification, TNM stage, lymph node metastasis, and distant metastasis (Supporting Information Table S3). Western blotting assays were conducted in 18 cases of CRLM patients, namely cohort 4. It was also observed that REEP6 expression was significantly enhanced in CRLM tissues compared to primary CRC tissues, and paired para-carcinoma tissues had the lowest REEP6 expression (Fig. 1L). Taken together, these results suggest that REEP6 is increased and correlated with a poor prognosis in CRC.

3.2. *REEP6 facilitates glycolysis and tumorigenesis in CRC*

To explore the dominant biological processes of CRC progression driven by REEP6, gene set enrichment analysis (GSEA) was performed in the TCGA database. The results exhibited a marked enrichment of the glycolysis pathway (Fig. 2A and Supporting Information Fig. S1A). Compared with NCM460, REEP6 was significantly upregulated in CRC cell lines, and moreover, DLD-1 and RKO cells had the highest expression levels (Fig. S1B and S1C). To verify whether abnormal glycolysis is mediated by REEP6, glucose uptake and lactate production were measured in CRC cell lines in which REEP6 expression was depleted or overexpression by a lentivirus-mediated transfection system. As shown in Fig. 2B and Fig. S1D, REEP6 deletion dramatically attenuated the glucose uptake and lactate production in DLD-1 and RKO cells, while ectopic REEP6 expression led to the opposite effects. Likewise, similar results were further validated by extracellular acidification rate (ECAR) assay, an indicator of overall glycolytic flux. The glycolytic rate and glycolytic capacity were impaired by knocking down *REEP6* in DLD-1 and RKO cells and enhanced when REEP6 was overexpressed (Fig. 2C and D, Fig. S1E and S1F). Collectively, these findings suggest that REEP6 promotes glycolysis in CRC cells.

Accumulating evidence has shown that aerobic glycolysis prominently fuels tumorigenesis and proliferation[33,34]. In consequence, we investigate whether REEP6 affects tumorigenesis and proliferation of CRC cells *in vitro* and *in vivo*. As expected, silencing REEP6 strikingly undermined the cell viability and colony formation capacity of DLD-1 and RKO cells, and upregulating REEP6 yielded an increased proliferation ability (Fig. S1G−S1I). The tumor-promoting role of REEP6 was further confirmed by CRC patient-derived organoid (PDO) models. Organoids' number and size were both reduced by lentivirus-mediated REEP6 depletion. In contrast, organoids stably overexpressing REEP6 markedly strengthened their growth ability (Fig. 2E−G).

Next, subcutaneous xenograft mouse models were established to assess the function of REEP6 in CRC tumorigenesis *in vivo*. *REEP6* knocking down or overexpressing DLD-1 cells and their corresponding control cells were inoculated into nude mice. Consistent with the above *in vitro* findings, DLD-1 cells stably depleted REEP6 developed tumors more slowly, with smaller tumor volumes and weights. While opposite outcomes were observed in DLD-1 cells with excessive expression of REEP6 (Fig. 2H and I). Recombinant adeno-associated virus serotypes 9 (AAV9) were excessively applied to intestinal disease study, for its relatively highly efficient gene transduction potential to intestinal epithelial cells[31,35,36]. *AAV-REEP6* knockdown (*AAV-REEP6*^{KD}), *AAV-REEP6* overexpression (*AAV-REEP6*^{OE}), and their corresponding control AAV (*AAV*^{shNC} or *AAV*^{vector}) were injected into 4-week-old male BALB/c mice through the tail vein. To confirm intestinal transfection efficiency, qRT-PCR and western blotting assays were employed to detect REEP6 expressions in colons (Supporting Information Fig. S2A and S2B). Azoxymethane and dextran sodium sulfate (AOM/DSS) models representing inflammation-induced tumorigenesis in CRC were combined with the AAV system to evaluate REEP6 in CRC tumorigenesis (Fig. 2J). AAV-REEP6^{KD} mice displayed notably fewer tumor numbers and smaller tumor sizes than their *AAV*^{shNC} mice (Fig. 2K and L). Moreover, increased survival rates were also observed in *AAV-REEP6*^{KD} mice rather than *AAV*^{shNC} mice (Fig. 2M). Consistently, AAV-REEP6^{KD} animals displayed a dramatic deficiency in tumor cell proliferation and a remarked increase in tumor cell apoptosis characterized by decreased proportions of Ki-67 staining and elevated proportions of TUNEL staining (Fig. S2C−S2E). Moreover, AAV-REEP6^{OE} mice exhibited opposite phenotypes in the abovementioned observational indicators compared to corresponding control mice (Fig. 2K−M, Fig. S2C−S2E). Together, these data illustrate that REEP6 facilitates CRC tumorigenesis *in vivo*.

3.3. *REEP6 interacts with PGAM1 and enhances PGAM1 enzyme activity*

Next, to uncover the underlying molecular mechanism by which REEP6 promotes glycolysis and tumorigenesis in CRC, co-immunoprecipitation (co-IP) coupled with protein mass spectrometry (MS) analyses found that the abundance of PGAM1 was prominent in REEP6-interacting proteins (Fig. 3A and Supporting Information Fig. S3A). Furthermore, PGAM1, known as a glycolytic enzyme in cancer metabolism, has been reported to be upregulated and enzymatically activated by many mechanisms[20,21]. The interaction between REEP6 and PGAM1 was further validated by endogenous and exogenous co-IP assays in DLD-1, RKO, and HEK-293T cells (Fig. 3B and C). Immunofluorescence (IF) analyses confirmed the cytoplasmic co-localization between REEP6 and PGAM1 in DLD-1 and RKO cells (Fig. 3D). Recombinant full-length GST-tagged REEP6 was generated for Glutathione S-transferase (GST) pull-down assay. The results showed that REEP6 is directly bound to PGAM1

interactions between PGAM1 and REEP6 *in vitro* with GST pull-down assays. Fusion protein beads were used for pull-down and detected with anti-Myc antibody ($n = 3$). (F) *REEP6* and *PGAM1* domain structure and deletion mutants designed for depicting the interacting domains. (G) The C-terminal domain (CTD: residues 109−211) of REEP6 interacted with PGAM1. HEK-293T cells were transfected with 2 μg Myc-tagged PGAM1 together with GFP-tagged REEP6 full-length or mutants. After 24 h, cell lysates were harvested and co-IP was performed using anti-GFP beads. The possible interacted REEP6 domains were detected by anti-Myc antibody ($n = 3$). (H) The truncated mutant 3 (TM3: residues 169−254) of *PGAM1* interacted with REEP6. HEK-293T cells were transfected with 2 μg GFP-tagged REEP6 together with Myc-tagged PGAM1 full-length or mutants. After 24 h, cell lysates were harvested and co-IP was performed using anti-Myc beads. The possible interacted PGAM1 domains were detected by anti-GFP antibody ($n = 3$).

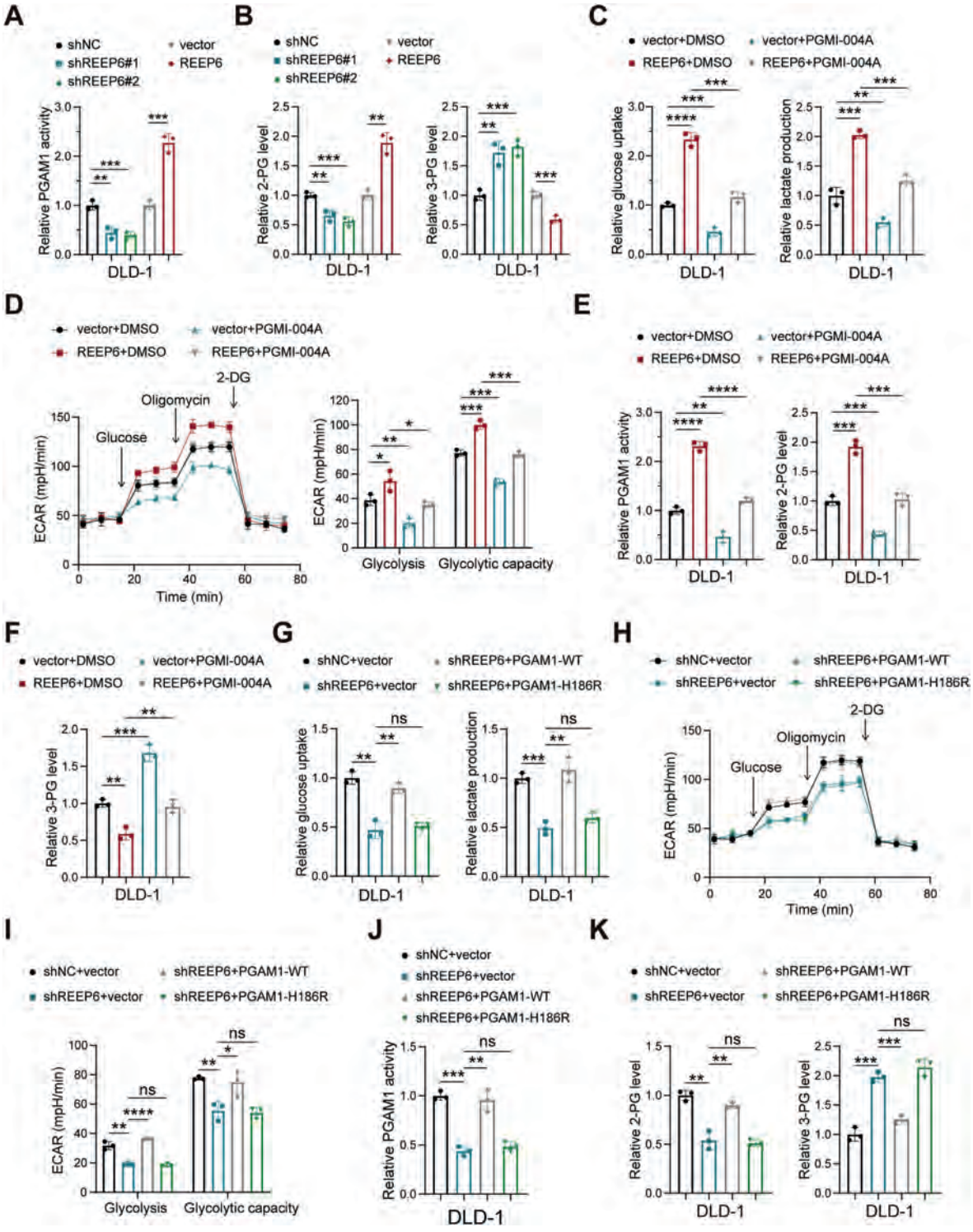

Figure 4 REEP6 enhances PGAM1 enzyme activity. (A) Relative PGAM1 activity was measured by PGAM1 activity assays in DLD-1 cells with the indicated lentiviruses transfection ($n = 3$). (B) Relative 2-PG and 3-PG levels were detected by ELISA assays in the indicated DLD-1 cells ($n = 3$). (C) Glucose uptake and lactate production were measured in the indicated DLD-1 cells. REEP6 stably overexpressed DLD-1 cells were treated with PGMI-004A ($n = 3$). (D) ECAR was measured in the indicated DLD-1 cells, and column statistics were shown in the right panel ($n = 3$). (E, F) Relative PGAM1 activity, 2-PG (E), and 3-PG levels (F) were detected in the DLD-1 cells which were stably overexpressed REEP6 in the presence or absence of PGMI-004A ($n = 3$). (G–I) Glucose uptake, lactate production (G), and ECAR (H, I) were analyzed in DLD-1 cells transfected with Lv-shREEP6 followed by PGAM1-WT and its mutant (PGAM1-H186R) plasmids ($n = 3$). (J, K) Relative PGAM1 activity (J), 2-PG and 3-PG levels (K) in DLD-1 cells transfected with Lv-shREEP6 followed by PGAM1-WT and its mutant (PGAM1-H186R) plasmids ($n = 3$). All data are presented as the mean ± SD. ns = no significance, $^{*}P < 0.05$, $^{**}P < 0.01$, $^{***}P < 0.001$, $^{****}P < 0.0001$. *P* values were determined by the two-tailed Student's *t*-tests (A)–(G) and (I)–(K).

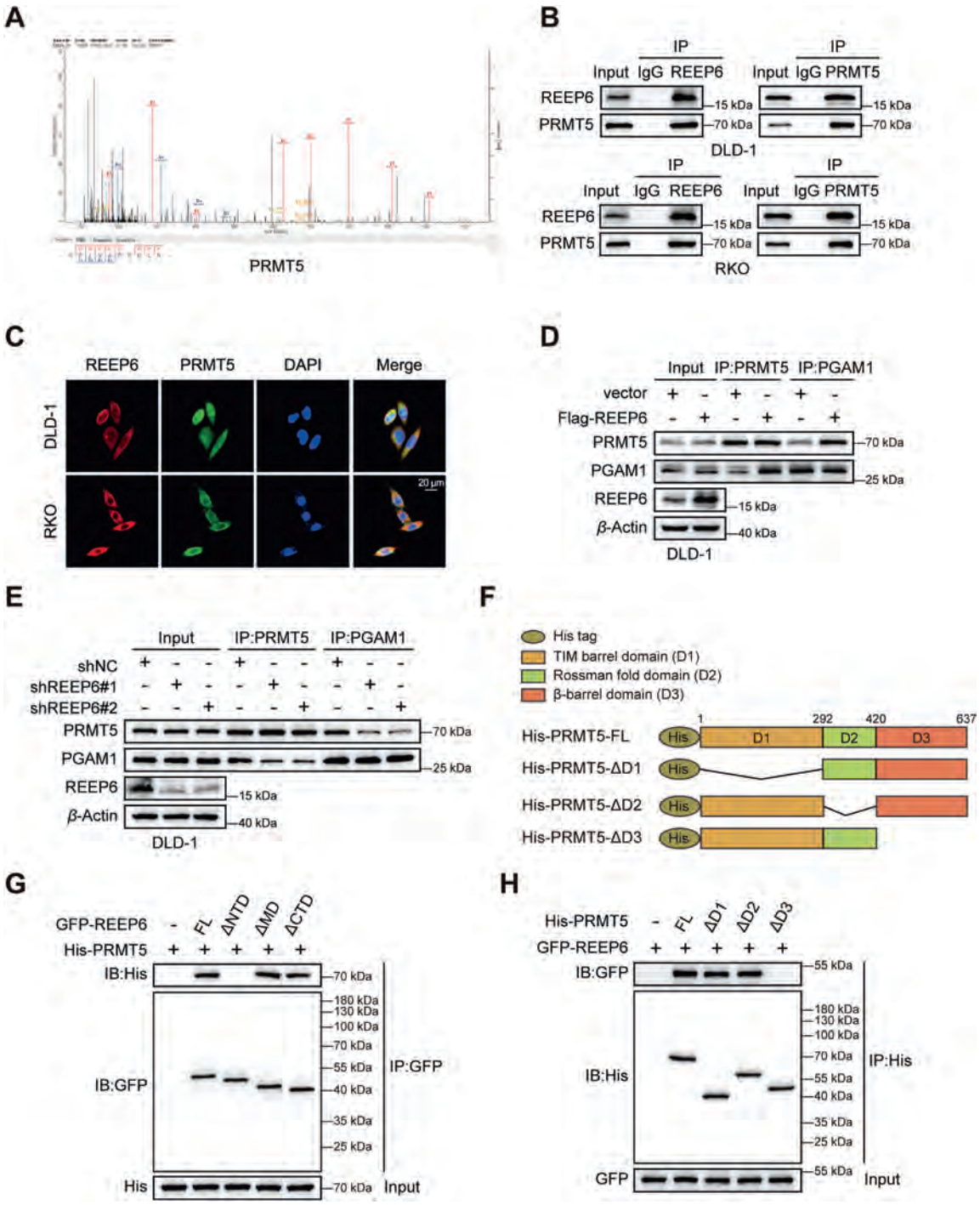

Figure 5 REEP6 interacts with PRMT5 and strengthens the PRMT5−PGAM1 complex. (A) Representative specific peptides of PRMT5 were identified by liquid chromatography tandem mass spectrometry (LC−MS/MS). (B) Mutual co-immunoprecipitation (co-IP) assays were performed to confirm the endogenous interaction between REEP6 and PRMT5 in DLD-1 and RKO cells ($n = 3$). (C) Immunofluorescence (IF) assays verified the cytoplasmatic co-localization of REEP6 and PRMT5 in DLD-1 and RKO cells (scale bars: 20 μm). (D, E) DLD-1 cells were stably transfected Lv-REEP6 or Lv-shREEP6 and then the cell lysis was harvested for quantified co-IP assay with anti-PRMT5 or anti-PGAM1 antibodies, followed by IB analysis ($n = 3$). (F) PRMT5 domain structure and deletion mutants designed for depicting the interacting domains. (G) The N-terminal domain (NTD: residues 1−42) of REEP6 interacted with PRMT5. HEK-293T cells were transfected with 2 μg His-tagged PRMT5 together with GFP-tagged REEP6 full-length or mutants. After 24 h, cell lysates were harvested and co-IP was performed using anti-GFP beads. The possible interacted REEP6 domains were detected by anti-His antibody ($n = 3$). (H) The β-barrel domain (D3: residues 420−637) of PRMT5 interacted with REEP6. HEK-293T cells were transfected with 2 μg GFP-tagged REEP6 together with His-tagged PRMT5 full-length or mutants. After 24 h, cell lysates were harvested and co-IP was performed using anti-His beads. The possible interacted PRMT5 domains were detected by anti-GFP antibody ($n = 3$).

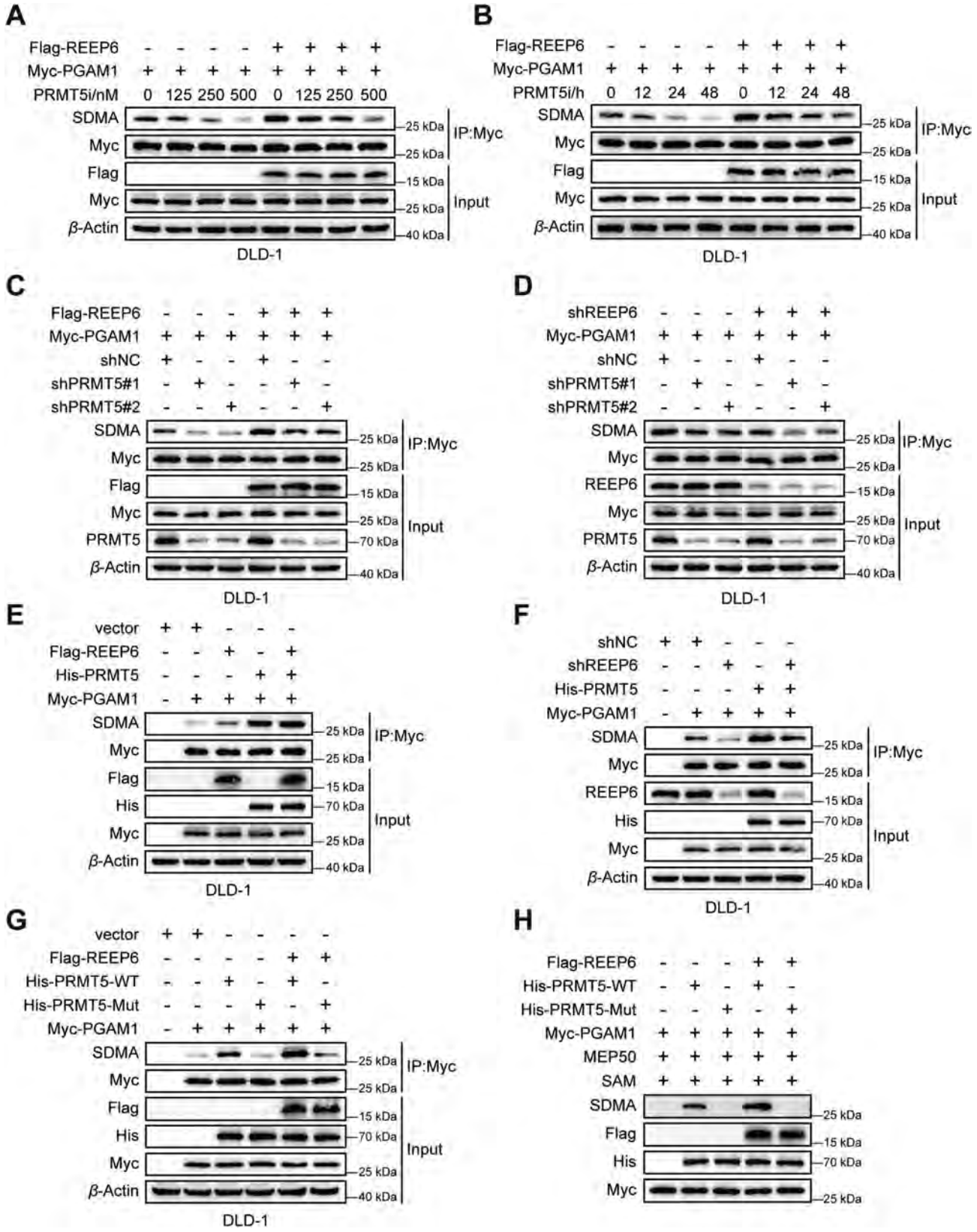

Figure 6 REEP6 promotes PRMT5 catalyzing symmetric dimethylation of PGAM1. (A, B) DLD-1 cells expressed Myc-tagged PGAM1, with or without Flag-tagged REEP6 were treated with PRMT5 inhibitor (GSK3326595) in a dosage-dependent manner for 24 h or a time-dependent manner with 250 nmol/L. Then Myc-tagged PGAM1 was immunoprecipitated with anti-Myc beads followed by immunoblotting analysis to detect the SDMA levels ($n = 3$). (C, D) DLD-1 cells were transfected with shPRMT5 plasmid and other indicated plasmids. Then, Myc-tagged PGAM1 was immunoprecipitated with anti-Myc beads followed by immunoblotting analysis to detect the SDMA levels ($n = 3$). (E, F) DLD-1 cells were

(Fig. 3E). A series of truncated mutants of *REEP6* and *PGAM1* was constructed to depict the interacting domains (Fig. 3F). The results demonstrated that the C-terminal domain (CTD: residues 109-211) of REEP6 physically interacted with the truncated mutant 3 (TM3: residues 169-254) of *PGAM1* (Fig. 3G and H). Moreover, it has been reported that PGAM1 interacts with ACTA2 to promote metastasis, which is not dependent on its metabolic functions[37]. We therefore investigate whether REEP6 interacts with PGAM1 through the ACTA2-binding motif independent of its metabolic activity. The results showed that overexpression of REEP6 in DLD-1 and RKO cells did not affect the binding between PGAM1 and ACTA2 (Fig. S3B). Furthermore, we constructed PGAM1 Δ201-210 deletions, which were verified to lose interaction with ATCA2, to examine its association with REEP6[37]. The results showed that PGAM1 Δ201−210 deletions still retained the interaction with REEP6 (Fig. S3C). These results collectively suggest that REEP6 interacts with PGAM1 independent of the ACTA2-binding motif.

We next wondered whether REEP6 modulates PGAM1 expression levels and enzymatic activity. qRT-PCR and western blotting showed that REEP6 failed to regulate the mRNA and protein levels of PGAM1 (Fig. S3D−S3F). However, the enzymatic activity of PGAM1 could be effectively crippled *via* stably introducing shREEP6 to DLD-1 and RKO cells and augmented when REEP6 was ectopically expressed (Fig. 4A and Supporting Information Fig. S3G). Moreover, the levels of PGAM1 enzymatic reaction substrate 3-PG and product 2-PG were measured by ELISA assays. Our data suggest that the depletion of REEP6 markedly reduced the levels of 2-PG and increased the levels of 3-PG in DLD-1 and RKO cells, and vice versa (Fig. 4B and Fig. S3G). Then, we preliminarily explored the expression level of PGAM1 in CRC patients of cohorts 1 and 2. As the results shown in Fig. S3H, there were no significant differences in the expression of PGAM1 mRNA between the tumor tissues and the adjacent normal tissues in cohort 1. Simultaneously, the IHC staining of CRC tissue microarrays in cohort 2 showed that the protein level of PGAM1 did not show significant differences either (Fig. S3I and S3J). These results suggest that PGAM1 exhibits a certain level of expression in CRC, which is functionally significant despite not being highly overexpressed.

A small molecule inhibitor (PGMI-004A) and an enzymatically inactive mutant (PGAM1-H186R) of *PGAM1* were introduced to confirm the role of PGAM1 enzyme activity in REEP6-mediated abnormal glycolysis[30,37]. Boosted glucose uptake, lactate production, glycolytic rate, and glycolytic capacity induced by REEP6 overexpression could be abolished by PGMI-004A treatment in DLD-1 and RKO cells (Fig. 4C and D, Supporting Information Fig. S4A and S4B). Moreover, treatment with PGMI-004A rescued the promoted PGAM1 enzymatic activity, increased 2-PG levels, and reduced 3-PG levels caused by REEP6 ectopic expression in DLD-1 and RKO cells (Fig. 4E and F, Fig. S4C). In consonance with these observations, decreased glucose uptake, lactate production, glycolytic rate and glycolytic capacity caused by REEP6 depletion could be rescued by the introduction of lentivirus-mediated wild-type PGAM1 expression but PGAM1-H186R failed (Fig. 4G−I, Fig. S4D and S4E). Furthermore, *REEP6* knockdown impaired PGAM1 enzymatic activity, decreased 2-PG levels, and increased 3-PG levels in DLD-1 and RKO cells, which could be abolished by wild-type PGAM1, but PGAM1-H186R had no significant effect (Fig. 4J and K, Fig. S4F and S4G). These data together suggest that REEP6 interacts with PGAM1 and promotes PGAM1 enzyme activity. More importantly, PGAM1, serving as a mutase in glycolysis, mediates the process of REEP6-enhanced glycolysis.

3.4. REEP6 strengthens the PRMT5-PGAM1 complex and promotes PRMT5 catalyzing symmetric dimethylation of PGAM1

Considering many researchers reported that the enzymatic activity of PGAM1 could be regulated by multiple kinds of post-translational modifications (PTMs), we presumed that REEP6 induced the increase in PGAM1 activity may be mediated by a type of PTM[21-23]. By interrogating REEP6 potentially interacting proteins, PRMT5 as a classical arginine methyltransferase is ranked third based on protein abundance, which aroused our interest (Figs. 3A and 5A). Furthermore, co-IP and GST pull-down assays confirmed the interaction between REEP6 and PRMT5 in CRC cells and HEK-293T cells (Fig. 5B, Supporting Information Fig. S5A and S5B). Confocal microscopy analysis of DLD-1 and RKO cells observed the co-localization between REEP6 and PRMT5 mainly in the cytoplasm (Fig. 5C). Indeed, we also found that REEP6 could not affect the mRNA and protein levels of PRMT5 (Fig. S5C−S5F). Moreover, PRMT5 did not regulate REEP6 or PGAM1 mRNA and protein expression (Fig. S5G−S5J). Next, we wondered whether REEP6 could act as a molecular scaffold to bridge and consolidate PRMT5 and PGAM1 interaction. Quantified co-IP experiments confirmed the interaction between PRMT5 and PGAM1, and the formation of this complex could be drastically cemented *via* REEP6 overexpression, whereas REEP6 depletion weakened it (Fig. 5D and E, Supporting Information Fig. S6A−S6C). Molecular domain mapping showed that the N-terminal domain (NTD: residues 1−43) of REEP6 and the β-barrel domain (D3: residues 420−637) located in PRMT5 mediated the interaction between REEP6 and PRMT5 (Fig. 5F−H). The Rossman fold domain (D2: residues 292−420) of PRMT5 and the truncated mutant 1 (TM1: residues 1−84) of *PGAM1* were responsible for the binding of PRMT5 and PGAM1 (Fig. S6D and S6E). Furthermore, GST pull-down assays demonstrated direct physical interaction between PRMT5 and PGAM1 (Fig. S6F). These data suggest that REEP6-PRMT5-PGAM1 forms a heterotrimeric complex in CRC.

We next examined whether PRMT5 plays an arginine methyltransferase role in the symmetric dimethylation of PGAM1 and whether REEP6 enhanced this catalytic reaction. Our results exhibited that the SDMA level of PGAM1 was prominently suppressed through PRMT5 inhibitor GSK3326595 treatment in a dose- and time-dependent manner in DLD-1 and RKO cells (Fig. 6A and B, Fig. S6G−S6L). More importantly, this effect was

overexpressed His-tagged PRMT5 and other indicated plasmids. Then, Myc-tagged PGAM1 was immunoprecipitated with anti-Myc beads followed by immunoblotting analysis to detect the SDMA levels ($n = 3$). (G) DLD-1 cells were transiently expressed His-tagged PRMT5 wild type (PRMT5-WT) or its inactive mutant (*PRMT5-G367A*/*R368A*) and other indicated plasmids. Then, Myc-tagged PGAM1 was immunoprecipitated with anti-Myc beads followed by immunoblotting analysis to detect the SDMA levels ($n = 3$). (H) An *in vitro* methylation assay was conducted to confirm the methylation of PGAM1 mediated by PRMT5, and REEP6 strengthens this enzymatic reaction. The reaction product was harvested for immunoblotting analysis to detect the levels of SDMA ($n = 3$).

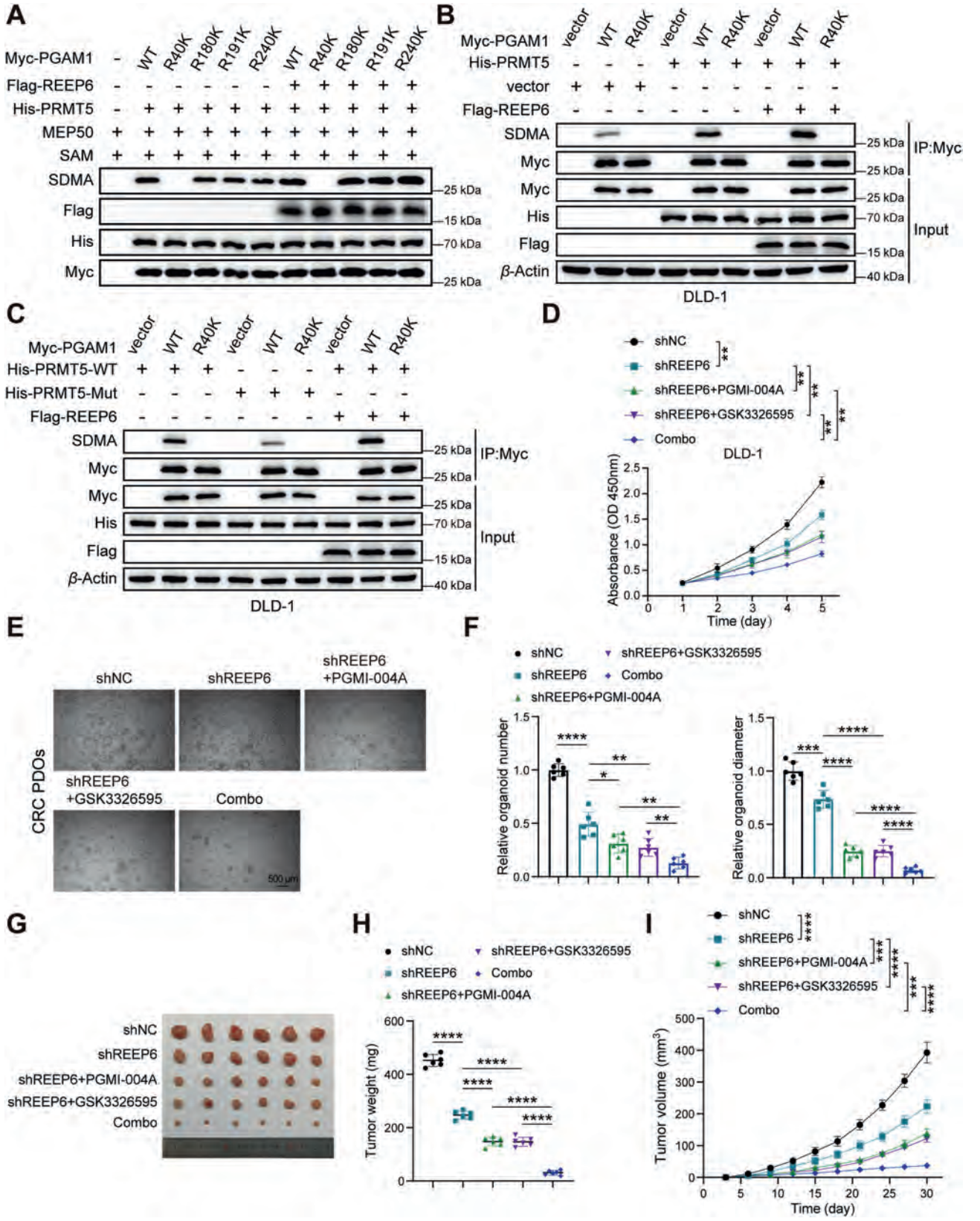

Figure 7 PRMT5 methylates PGAM1 at R40, and the combined treatment targeting REEP6−PRMT5−PGAM1 complex exhibits anti-tumor effects. (A) An *in vitro* methylation assay was performed to verify the meth−ylation of PGAM1 mediated by PRMT5 at R40, and REEP6 promotes this enzymatic reaction. Myc-tagged wild-type PGAM1 (PGAM1 WT) or its mutants were transiently expressed in HEK-293T cells and purified by immunoprecipitation using anti-Myc beads. Methylation of PGAM1 by recombinant human His-tagged PRMT5, MEP50, and Flag-tagged REEP6 was detected by Western blotting using an anti-symmetric dimethyl arginine antibody ($n = 3$). (B) *In vivo* methylation assays

reinforced by REEP6 overexpression, while abated by REEP6 depletion (Fig. 6A and B, Fig. S6G−S6L). Genetical inhibition of PRMT5 notably reduced the SDMA modification of PGAM1 and genetical introduction of PRMT5 facilitated PGAM1 methylation (Fig. 6C−F and Supporting Information Fig. S7A−S7D). On this basis, REEP6 overexpression strengthened and *REEP6* knockdown weakened the SDMA of PGAM1 mediated by PRMT5 in DLD-1 and RKO cells (Fig. 6C−F and Fig. S7A−S7D). Similarly, the enzyme inactive mutant of *PRMT5* (*PRMT5-G367A*/*R368A*) failed to catalyze the SDMA modification of PGAM1 compared to wild-type *PRMT5* (Fig. 6G and Fig. S7E−S7G). Moreover, the promotion effect of REEP6 on PGAM1 methylation catalyzed by wild-type *PRMT5* was also observed whereas it was difficult to detect the SDMA of PGAM1 mediated by PRMT5-G367A/R368A (Fig. 6G and Fig. S7E−S7G). Through an i*n vitro* methylation assay, we also validated that the enzymatic activity of PRMT5 was essential for SDMA modification of PGAM1, and REEP6 could intensify this enzymatic reaction (Fig. 6H). Next, to investigate whether PRMT5 catalyzes SDMA modification on REEP6, co-IP assays were performed in HEK-293T cells. As shown in Fig. S7H, no SDMA signals were detected on REEP6 proteins when PRMT5 was ectopically expressed. In conclusion, these data indicate that REEP6 strengthens the formation of PRMT5−PGAM1 complex and further promotes PRMT5 catalyzing PGAM1 symmetric dimethylation.

3.5. REEP6 increased PGAM1 enzymatic activity is mediated by arginine methyltransferase PRMT5

We further investigated whether PRMT5 serving as an arginine methyltransferase could regulate enhanced PGAM1 enzymatic activity mediated by REEP6. Pharmacological or genetic elimination of PRMT5 obviously reversed the elevated glucose uptake, lactate production, glycolytic rate, and glycolytic capacity caused by ectopic expression of REEP6 in CRC cell lines (Supporting Information Fig. S8A−S8H). What's more, improved PGAM1 enzymatic activity, elevated 2-PG levels, and declined 3-PG levels mediated by REEP6 could be partially abolished by PRMT5 inhibition (Supporting Information Fig. S9A−S9D). Consistent with these results, overexpression of PRMT5-WT rescued the impaired glucose uptake, lactate production, glycolytic rate, and glycolytic capacity mediated by stable depletion of REEP6 in DLD-1 and RKO cells, while catalytic inactive mutant *PRMT5-G367A*/*R368A* was incapable of doing it (Fig. S9E−S9H). Similarly, *PRMT5-WT* but not *PRMT5-G367A*/*R368A* rescued the weakened PGAM1 enzymatic activity, reduced 2-PG levels, and increased 3-PG levels caused by *REEP6* knockdown in DLD-1 and RKO cells (Fig. S9I and S9J). In summary, the catalytic activity of PRMT5 as an arginine methyltransferase is essential for increasing PGAM1 enzymatic activity mediated by REEP6.

3.6. REEP6 enhances PRMT5 catalyzing the symmetric dimethylation of PGAM1 at R40

To identify the exact arginine residues of PGAM1 SDMA modification, GPS-MSP and PRmePred were applied to predict the candidate arginine residues in PGAM1 (Supporting Information Fig. S10A and S10B)[38-40]. Then, wild-type *PGAM1* (*PGAM1-WT*) and its mutants in which specific arginine was substituted by lysine (termed R40K, R180K, R191K, and R240K) were generated. *In vitro* methylation assay illustrated that *PGAM1-R40K* mutant clearly abolished methylation in PGAM1 mediated by recombinant PRMT5 and REEP6 failed to strengthen the SDMA level in *PGAM1-R40K* mutant (Fig. 7A). Then, *PGAM1-WT* and four mutants were transiently transfected to HEK-293T cells. Similar results were also observed in the *in vivo* methylation assay (Supporting Information Fig. S11A). Subsequently, we further verified whether the residue R40 of PGAM1 was dimethylated symmetrically in CRC cell lines and *in vitro*. The result showed that REEP6 obviously facilitated the SDMA level of PGAM1-WT which is catalyzed by PRMT5, whereas PGAM1-R40K completely eliminated it (Fig. 7B, Fig. S11B and S11C). More importantly, we also demonstrated that the enzymatic activity of PRMT5 is indispensable for the methylation of *PGAM1* at *R40* (Fig. 7C and Fig. S11D). Collectively, these data indicated that PRMT5 dimethylates symmetrically PGAM1 at R40, and REEP6 dramatically enhanced this catalytic reaction.

Considering REEP6-PRMT5-PGAM1 heterotrimeric complex promoted glycolysis in CRC cells, we detected whether combined inhibition of this ternary complex could yield a better therapeutic effect in CRC. GSK3326595 and PGMI-004A both effectively suppressed CRC cell lines and PDO proliferation in concentration-dependent effects, and the IC_{50} values were calculated (Fig. S11E and S11F). Next, our results showed that combined targeting REEP6-PRMT5-PGAM1 prominently impeded the cell proliferation and colony formation capacities of DLD-1 and RKO cells compared to single or two treatments (Fig. 7D and Fig. S11G−S11I). A similar phenomenon with an inhibitory organoid number and size was also observed in CRC PDO models (Fig. 7E and F). DLD-1 cell-derived xenograft models with stably depleted REEP6 were also applied to test the synergistic effect of this combined treatment. Compared with single or two treatments with shREEP6, GSK3326595, or PGMI-004A, combined three treatments with shREEP6, GSK3326595, and PGMI-004A dramatically inhibited xenograft growth (Fig. 7G−I). Collectively, the above data suggest that the combined targeting of

were conducted in DLD-1 cells. The indicated plasmids were transiently transfected to DLD-1 cells. Myc-tagged PGAM1 was immunoprecipitated with anti-Myc beads followed by immunoblotting analysis using an anti-symmetric dimethyl arginine antibody ($n = 3$). (C) The enzymatic activity of PRMT5 is indispensable for the methylation of PGAM1 at R40 in DLD-1 cells. His-tagged *PRMT5* wild type (*PRMT5-WT*) or its inactive mutant (*PRMT5-G367A*/*R368A*) and other indicated plasmids were transiently expressed in DLD-1 cells. Myc-tagged PGAM1 was immunoprecipitated with anti-Myc beads followed by immunoblotting analysis using an anti-symmetric dimethyl arginine antibody ($n = 3$). (D) Cell counting kit-8 (CCK-8) assay was used to detect the cell viability in DLD-1 cells for each indicated treatment ($n = 3$). (E, F) The representative images (E) scale bars: 500 μm) and the relative organoid number or diameter (F) in CRC patient-derived organoid (PDO) for each indicated treatment ($n = 6$). (G−I) Representative images (G) and statistical analyses (H, I) of the xenograft tumors in nude mice bearing DLD-1 cells for each indicated treatment. When tumors were visible, tumor volumes were measured every 3 days. Tumors were harvested, photographed, and weighed on Day 30. $n = 6$ mice per group. All data are presented as the mean ± SD. $^{*}P < 0.05$, $^{**}P < 0.01$, $^{***}P < 0.001$, $^{****}P < 0.0001$. *P* values were determined by the two-tailed Student's *t*-tests (D, F, H, and I).

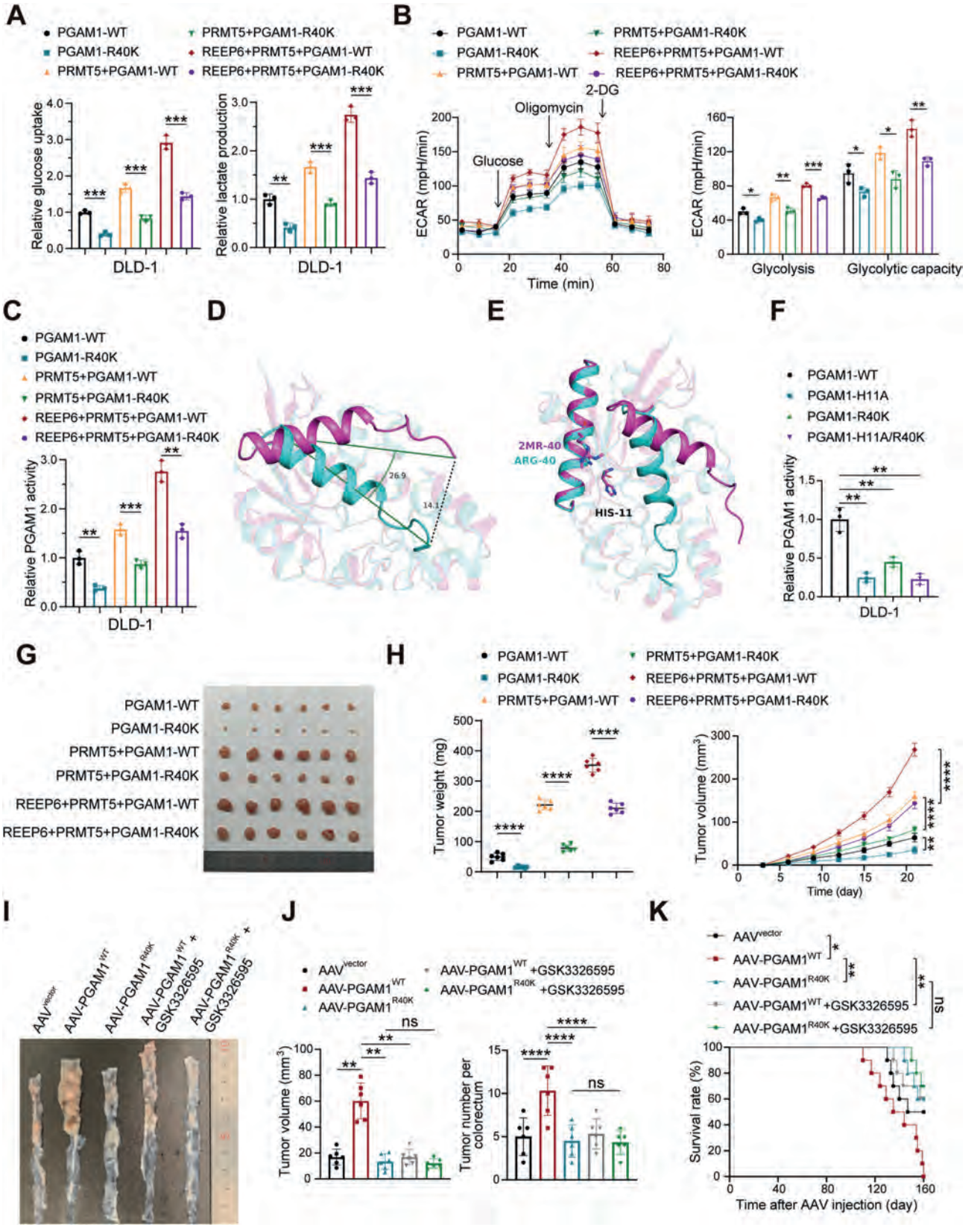

Figure 8 SDMA of PGAM1 at R40 promotes glycolysis and tumorigenesis in CRC. (A, B) Glucose uptake, lactate production (A), and ECAR (B) were detected in DLD-1 cells stably transfected with the indicated lentiviruses ($n = 3$). (C) Relative PGAM1 activity was measured by PGAM1 activity assays in DLD-1 cells with the indicated lentiviruses transfection ($n = 3$). (D) Diagram illustrating the conformational deflection in C-terminal α-helix (residues 232−254) of PGAM1 induced by R40me2s. The wild-type *PGAM1* is colored sky blue; pink indicates R40-symmetrically dimethylated PGAM1. (E) Conformational expansion at the H11 phosphorylation pocket entrance in PGAM1. (F) Relative

REEP6−PRMT5−PGAM1 complex possesses anti-tumor potential in CRC.

3.7. SDMA of PGAM1 at R40 promotes glycolysis and tumorigenesis in CRC

Next, we investigated whether PGAM1 SDMA affects its enzymatic activity, glycolysis, and tumorigenesis in CRC. Firstly, DLD-1 and RKO cells expressing *PGAM1-WT* but not *PGAM1-R40K* mutant showed stronger ability in glucose uptake, lactate production, glycolytic rate, and glycolytic capacity (Fig. 8A and B, Supporting Information Fig. S12A and S12B). Moreover, compared to *PGAM1-WT*, undermined PGAM1 enzymatic activity, reduced 2-PG levels, and increased 3-PG levels were detected in cell lines with PGAM1-R40K ectopic expression (Fig. 8C, Fig. S12C and S12D). In addition, REEP6/PRMT5 overexpression in CRC cell lines which is expressing *PGAM1-WT* significantly promoted glycolysis and enzymatic activity of PGAM1, while PGAM1-R40K impaired this effect (Fig. 8A−C, Fig. S12A−S12D). Next, the reason why methylated PGAM1 enhanced its activity as a glycolytic enzyme was further explored. The current consensus is that the enzymatic activity of PGAM1 is derived from the phosphorylation of histidine 11 (H11)[41,42]. Therefore, we speculated that SDMA of PGAM1 at R40 might change the three-dimensional conformation of PGAM1, rendering subsequent enhanced H11 phosphorylation. AlphaFold v3 and PyMOL2.6.0 were employed to investigate the potential mechanism by which symmetric dimethylarginine at R40 (R40me2s) enhances phosphorylation of histidine 11 (H11) in PGAM1 (Fig. S12E) [43]. As shown in Fig. 8D, R40me2s induces a conformational deflection in the C-terminal α-helix (residues 232−254) of PGAM1, resulting in a displacement of 14.1 Å and a bending angle of 26.9°. This structural rearrangement enlarges the entrance of the H11 phosphorylation pocket, which is formed by two α-helices (residues 30−49 and 232−254) (Fig. 8E). The increased cavity volume enhances the contact area and binding opportunities between PGAM1 and its upstream kinase. Furthermore, the extended side chain of R40me2s stabilizes the pocket entrance. Therefore, we speculate that the alteration in cavity volume caused by the R40me2s enhances the phosphorylation of H11 in PGAM1. In order to verify our speculation, we transfected a series of *PGAM1* point mutants into CRC cells. The results showed that compared with wild-type *PGAM1*, mutating *R40* to lysine (PGAM1-R40K) abolished SDMA signals and significantly weakened phosphorylation signals at H11 (Fig. S12F). Consistent with this, *PGAM1-R40K* and *H11A* mutants showed a remarked deficiency in enzymatic activity (Fig. 8F and Fig. S12G).

Then, we further evaluated the impact of PGAM1 SDMA on CRC tumorigenesis and proliferation *in vitro* and *in vivo*. PGAM1-WT but not PGAM1-R40K exhibited pronouncedly promoted effects on cell viability and colony formation capacity in DLD-1 and RKO cells (Supporting Information Figs. S12H, S12I, and S13A, S13B). Moreover, PGAM1-WT drastically enhanced cell viability and colony formation capacity in the presence of REEP6/PRMT5 ectopic expression, but not so much in the *PGAM1-R40K* mutant (Figs. S12H, S12I, and S13A, S13B). Subsequently, CRC PDO models and subcutaneous xenograft models further confirmed the above *in vitro* results (Fig. S13C and S13D, Fig. 8G and H). The AAV gene delivery system combined with AOM/DSS models was employed to validate the effect of PGAM1 SDMA on CRC tumorigenesis. Mice from the *AAV-PGAM1*^{WT} group had elevated tumor numbers and enhanced tumor volumes than their *AAV*^{vector} mice, whereas *AAV-PGAM1*^{R40K} prominently whittled this effect down (Fig. 8I and J). What's more, the *AAV-PGAM1*^{WT} group rather than *AAV*^{vector} mice, showed a crippled survival rate, and *PGAM1-R40K* mutant dramatically improved it (Fig. 8K). Meanwhile, we also found that proliferation potential which is characterized by Ki67 positive nuclei staining was increased, while apoptosis proportions quantified by the intensity of TUNEL staining were diminished in the *AAV-PGAM1*^{WT} group rather than their AAV^{vector} or AAV-PGAM1^{R40K} mice (Fig. S13E−S13G). More than that, GSK3326595 treatment could obviously impede AOM/DSS-induced tumorigenesis in *AAV-PGAM1*^{WT}, but the effect was weaker in *AAV-PGAM1*^{R40K} mice (Fig. 8I−K, Fig. S13E−S13G).

4. Discussion

The aberrant expression of REEP6 was reported in many cancers and its cancer-promoting role was illustrated by some researchers[25-27]. But REEP6 initially acts as a receptor expression-enhancing protein, the expression pattern and the new function of cancer glycolysis remain largely unknown in CRC. Here, our study reported that REEP6 is significantly elevated in CRC tissues compared to normal tissues. More importantly, CRC patients with high REEP6 expression indicated worse clinicopathological features and a poorer overall survival rate in our cohorts. Our results confirmed that REEP6 fueled the cell proliferation and tumorigenesis in CRC cells which was caused by the enhanced glycolytic flux. Even so, the exact mechanism implicated in the upregulation of REEP6 in CRC cells needs further exploration. The integration of nanotechnology (including lipid nanoparticles, polymer nanoparticles, and bioinspired vectors) combined with RNA interference (RNAi) has emerged as an innovative approach for cancer targeting therapy[44-46]. Given the aberrant expression and the cancer-promoting role of REEP6, it will be a promising avenue for CRC therapeutic strategy that the utilization of nanoparticles delivered siRNA targeting REEP6.

In this study, we demonstrated that REEP6 serving as a molecular scaffold contributed to the formation of the PRMT5−PGAM1 complex. Furthermore, the formation of REEP6−PRMT5−PGAM1 ternary complex promoted PRMT5-

PGAM1 activity was measured by PGAM1 activity assays in DLD-1 cells with the indicated plasmids transfection ($n = 3$). (G, H) DLD-1 cells were subcutaneously injected into the flanks of nude mice after infecting the indicated lentiviruses. When tumors were visible, tumor volumes were measured every 3 days (H, right panel). Tumors were harvested, photographed (G), and weighed (H, left panel) on Day 21. $n = 6$ mice per group. (I) The colorectums were opened longitudinally, and representative colorectal images were derived from the indicated mice treated with AOM/DSS-induced CRC models. The indicated adeno-associated viruses (AAVs) were injected into the tail veins of BALB/c mice, followed by AOM/DSS chemically induced CRC, and then the mice were intraperitoneally administrated with DMSO or GSK3326595 100 mg/kg every 3 days. After 4 weeks, all mice were euthanatized. (J) Tumor volumes and tumor numbers were calculated in each group. $n = 6$ mice per group. (K) Survival curves for the indicated mice. $n = 10$ mice per group. All data are presented as the mean ± SD. ns = no significance, $^{*}P < 0.05$, $^{**}P < 0.01$, $^{***}P < 0.001$, $^{****}P < 0.0001$. *P* values were determined by the two-tailed Student's *t*-tests (A−C, F, H, and J), and Kaplan−Meier log-rank test (K).

mediated SDMA of PGAM1 at R40, which dramatically increased PGAM1 enzymatic activity in glycolysis. PRMT5 has been reported as an essential protein arginine methyltransferase involved in multiple non-metabolic pathways during CRC progression, which implicates several cellular processes such as epithelial-mesenchymal transition (EMT), ferroptosis, and histone modification[9,10,47-49]. Zhu et al.[47] reported that the inhibition of PRMT5 enhances irinotecan sensitivity, inducing the release of cytosolic double-stranded DNA, then activating the cGAS−STING signaling pathway, thereby enhancing anti-tumor immunotherapy for CRC patients with microsatellite stable state. This study emphasizes the novel role of PRMT5 as a DNA damage repair-related epigenetic gene in enhancing chemotherapy and immunotherapy sensitivity. In addition, PRMT5 has been demonstrated to regulate the AKT/mTOR signaling pathway through arginine methylation of AKT1, which participates in colorectal cancer liver metastasis[48]. Moreover, PRMT5 directly catalyzes symmetric demethylation of AlkB homologue 5 (ALKBH5) at Arg316 or inhibits ALKBH5 transcription by mediating symmetric dimethylation of histone residues (H4R3me2s and H3R8me2s). These actions aggravate CRC progression by facilitating immune evasion or attenuating ferroptosis, respectively[10,49]. It is necessary to recognize that these non-metabolic pathways may have synergistic or independent effects with our study on the metabolic axis. The therapeutic strategy of inhibiting PRMT5 activity may simultaneously target metabolic and non-metabolic pathways in CRC patients.

Most importantly, our report found that combined treatment targeting the REEP6−PRMT5−PGAM1 heterotrimeric complex showed a synergistic effect on anti-tumor tactics. For suppressing the enzymatic activity of PGAM1 in glycolysis, a series of inhibitors, including PGMI-004A, HK99, and KH3 have been developed in cancer treatment[30,50-52]. Among these, PGMI-004A, a potent PGAM1 inhibitor with an IC_{50} of 13.1 μmol/L, showed remarkable anti-tumor potential in xenograft mice *in vivo*, and in various human malignant tumor cells *in vitro*[30]. Next, as a potent and highly specific small-molecule inhibitor, GSK3326595 targeting the catalytic site of PRMT5 was also applied in the combined treatment[39,53]. GSK3326595 has shown a markedly antitumor and a favorable prognostic efficiency against some solid tumors and hematological malignant tumors in phase I/II clinical trials (NCT04676516, NCT03614728, and NCT02783300). Our report indicated that compared with single or two treatments with shREEP6, GSK3326595, or PGMI-004A, combined three treatments with shREEP6, GSK3326595, and PGMI-004A obviously impeded the growth and tumorigenesis in CRC cell lines, CRC PDO models, and xenograft models. This result paves the way for the combination targeting therapies that may provide a more promising strategy for CRC treatment. However, it should be noted that further validation through animal studies and subsequent clinical trials is essential for this combination therapy strategy.

5. Conclusions

Our study identified that REEP6 is significantly upregulated in CRC tissues and correlated with a poor prognosis in CRC patients. REEP6 promotes aerobic glycolysis and tumorigenesis in CRC both *in vitro* and *in vivo*. Mechanistically, REEP6 strengthens the PRMT5−PGAM1 complex and promotes PRMT5-mediated SDMA of PGAM1 at R40 residues. The methylated PGAM1 dramatically enhances its enzymatic activity and therefore boosts glycolytic flux in CRC cells. More than that, combined treatment targeting the REEP6−PRMT5−PGAM1 complex exhibit synergistic anti-tumor efficacy in CRC, which may present a novel and efficacious therapeutic strategy for CRC treatment.

Acknowledgments

We would like to thank the Core Facility of the First Affiliated Hospital of Nanjing Medical University for its help in the detection of experimental samples. This work was supported by the National Natural Science Foundation (Grant Numbers 82273406 and 82304221, China); Basic Research Program of Jiangsu Province (BK20221415 and BK20230730, China); Jiangsu Key Medical Discipline (General Surgery; Grant No. ZDXK202222, China); and Youth Program of the National Natural Science Foundation (Grant Numbers 82203768, China).

Author contributions

Yueming Sun and Tuo Wang generated the hypothesis and designed the experiments. Tuo Wang, Dongsheng Zhang, Chi Jin, and Hengjie Xu performed experiments. Tuo Wang performed animal experiments. Tuo Wang interpreted the data. Tuo Wang wrote the manuscript. Yueming Sun supervised the overall research, secured funding, and interpreted results. The author(s) read and approved the final manuscript.

Ethics statement

Human tissue study is approved by the committee on the ethics of The First School of Clinical Medicine, Nanjing Medical University and all patients endorsed informed consent. All animal experiments are conducted with the approval of the Committee on the Ethics of Animal Experiments of Nanjing Medical University. The ethical number of the animal experiment is IACUC-2403048.

Conflicts of interest

The authors declare no conflicts of interest.

Appendix A. Supplementary information

Supporting Information to this article can be found online at https://doi.org/10.1016/j.apsb.2025.10.025.

References

1. Eng C, Yoshino T, Ruíz-García E, Mostafa N, Cann CG, O'Brian B, et al. Colorectal cancer. *Lancet* 2024;**404**:294−310.
2. Bray F, Laversanne M, Sung H, Ferlay J, Siegel RL, Soerjomataram I, et al. Global cancer statistics 2022: GLOBOCAN estimates of incidence and mortality worldwide for 36 cancers in 185 countries. *CA Cancer J Clin* 2024;**74**:229−63.
3. Hanahan D, Weinberg RA. Hallmarks of cancer: the next generation. *Cell* 2011;**144**:646−74.
4. Vernieri C, Casola S, Foiani M, Pietrantonio F, de Braud F, Longo V. Targeting cancer metabolism: dietary and pharmacologic interventions. *Cancer Discov* 2016;**6**:1315−33.
5. Xiao Y, Yu TJ, Xu Y, Ding R, Wang YP, Jiang YZ, et al. Emerging therapies in cancer metabolism. *Cell Metab* 2023;**35**:1283−303.
6. Tufail M, Jiang CH, Li N. Altered metabolism in cancer: insights into energy pathways and therapeutic targets. *Mol Cancer* 2024;**23**:203.

7. Hwang JW, Cho Y, Bae GU, Kim SN, Kim YK. Protein arginine methyltransferases: promising targets for cancer therapy. *Exp Mol Med* 2021;**53**:788−808.
8. Zheng J, Li B, Wu Y, Wu X, Wang Y. Targeting arginine methyltransferase PRMT5 for cancer therapy: updated progress and novel strategies. *J Med Chem* 2023;**66**:8407−27.
9. Liu A, Yu C, Qiu C, Wu Q, Huang C, Li X, et al. PRMT5 methylating SMAD4 activates TGF-β signaling and promotes colorectal cancer metastasis. *Oncogene* 2023;**42**:1572−84.
10. Meng S, Liu H, Xu J, Deng C, Qian X, Chu S, et al. *PRMT5-mediated ALKBH5 methylation promotes colorectal cancer immune evasion via increasing CD276 expression*, **8**. Research (Wash D C); 2025. p. 549.
11. Vander Heiden MG, Cantley LC, Thompson CB. Understanding the warburg effect: the metabolic requirements of cell proliferation. *Science* 2009;**324**:1029−33.
12. Fendt SM. 100 years of the warburg effect: a cancer metabolism endeavor. *Cell* 2024;**187**:3824−8.
13. Zhong X, He X, Wang Y, Hu Z, Huang H, Zhao S, et al. Warburg effect in colorectal cancer: the emerging roles in tumor microenvironment and therapeutic implications. *J Hematol Oncol* 2022;**15**:160.
14. Li F, Si W, Xia L, Yin D, Wei T, Tao M, et al. Positive feedback regulation between glycolysis and histone lactylation drives oncogenesis in pancreatic ductal adenocarcinoma. *Mol Cancer* 2024;**23**:90.
15. Yang GJ, Tao F, Zhong HJ, Yang C, Chen J. Targeting PGAM1 in cancer: an emerging therapeutic opportunity. *Eur J Med Chem* 2022; **244**:114798.
16. Fothergill-Gilmore LA, Watson HC. The phosphoglycerate mutases. *Adv Enzymol Relat Area Mol Biol* 1989;**62**:227−313.
17. Chen G, Gharib TG, Wang H, Huang CC, Kuick R, Thomas DG, et al. Protein profiles associated with survival in lung adenocarcinoma. *Proc Natl Acad Sci U S A* 2003;**100**:13537−42.
18. Dong JK, Lei HM, Liang Q, Tang YB, Zhou Y, Wang Y, et al. Overcoming erlotinib resistance in *EGFR* mutation-positive lung adenocarcinomas through repression of phosphoglycerate dehydrogenase. *Theranostics* 2018;**8**:1808−23.
19. Zheng Y, Wang Y, Lu Z, Wan J, Jiang L, Song D, et al. PGAM1 inhibition promotes HCC ferroptosis and synergizes with anti-PD-1 immunotherapy. *Adv Sci (Weinh)* 2023;**10**:e2301928.
20. Qiu Z, Wang C, Huang P, Yuan Y, Shi Y, Lin Z, et al. RFX6 facilitates aerobic glycolysis-mediated growth and metastasis of hepatocellular carcinoma through targeting PGAM1. *Clin Transl Med* 2023;**13**: e1511.
21. Hitosugi T, Zhou L, Fan J, Elf S, Zhang L, Xie J, et al. Tyr26 phosphorylation of PGAM1 provides a metabolic advantage to tumours by stabilizing the active conformation. *Nat Commun* 2013;**4**:1790.
22. Yang G, Yuan Y, Yuan H, Wang J, Yun H, Geng Y, et al. Histone acetyltransferase 1 is a succinyltransferase for histones and nonhistones and promotes tumorigenesis. *EMBO Rep* 2021;**22**:e50967.
23. Hallows WC, Yu W, Denu JM. Regulation of glycolytic enzyme phosphoglycerate mutase-1 by Sirt1 protein-mediated deacetylation. *J Biol Chem* 2012;**287**:3850−8.
24. Fan S, Liu H, Li L. The REEP family of proteins: molecular targets and role in pathophysiology. *Pharmacol Res* 2022;**185**:106477.
25. Park CR, You DJ, Park S, Mander S, Jang DE, Yeom SC, et al. The accessory proteins REEP5 and REEP6 refine CXCR1-mediated cellular responses and lung cancer progression. *Sci Rep* 2016;**6**:39041.
26. Xia L, Wang H, Du G, Cheng X, Zhang R, Yu H, et al. Receptor accessory protein 6, a novel ferroptosis suppressor, drives oral squamous cell carcinoma by maintaining endoplasmic reticulum hemostasis. *Int J Biol Macromol* 2024;**283**:137565.
27. Tseng CC, Hung CC, Shu CW, Lee CH, Chen CF, Kuo MS, et al. The clinical and biological effects of receptor expression-enhancing orotein 6 in tongue squamous cell carcinoma. *Biomedicines* 2023;**11**: 1270.
28. Zhang Z, Li J, Huang Y, Peng W, Qian W, Gu J, et al. Upregulated miR-1258 regulates cell cycle and inhibits cell proliferation by directly targeting E2F8 in CRC. *Cell Prolif* 2018;**51**:e12505.
29. Hou Y, Zhang X, Yao H, Hou L, Zhang Q, Tao E, et al. METTL14 modulates glycolysis to inhibit colorectal tumorigenesis in *p53*-wild-type cells. *EMBO Rep* 2023;**24**:e56325.
30. Hitosugi T, Zhou L, Elf S, Fan J, Kang HB, Seo JH, et al. Phosphoglycerate mutase 1 coordinates glycolysis and biosynthesis to promote tumor growth. *Cancer Cell* 2012;**22**:585−600.
31. Polyak S, Mach A, Porvasnik S, Dixon L, Conlon T, Erger KE, et al. Identification of adeno-associated viral vectors suitable for intestinal gene delivery and modulation of experimental colitis. *Am J Physiol Gastrointest Liver Physiol* 2012;**302**:G296−308.
32. Neufert C, Becker C, Neurath MF. An inducible mouse model of colon carcinogenesis for the analysis of sporadic and inflammation-driven tumor progression. *Nat Protoc* 2007;**2**:1998−2004.
33. Wang RH, Chen PR, Chen YT, Chen YC, Chu YH, Chien CC, et al. Hydrogen sulfide coordinates glucose metabolism switch through destabilizing tetrameric pyruvate kinase M2. *Nat Commun* 2024;**15**: 7463.
34. Chen T, Xie S, Cheng J, Zhao Q, Wu H, Jiang P, et al. AKT1 phosphorylation of cytoplasmic ME2 induces a metabolic switch to glycolysis for tumorigenesis. *Nat Commun* 2024;**15**:686.
35. Fang Y, Shen ZY, Zhan YZ, Feng XC, Chen KL, Li YS, et al. CD36 inhibits β-catenin/c-myc-mediated glycolysis through ubiquitination of GPC4 to repress colorectal tumorigenesis. *Nat Commun* 2019;**10**: 3981.
36. Hua F, Shang S, Yang YW, Zhang HZ, Xu TL, Yu JJ, et al. TRIB3 interacts with β-catenin and TCF4 to increase sstem cell features of colorectal cancer stem cells and tumorigenesis. *Gastroenterology* 2019;**156**:708-21.e15.
37. Zhang D, Jin N, Sun W, Li X, Liu B, Xie Z, et al. Phosphoglycerate mutase 1 promotes cancer cell migration independent of its metabolic activity. *Oncogene* 2017;**36**:2900−9.
38. Abe Y, Sano T, Otsuka N, Ogawa M, Tanaka N. PRMT5-mediated methylation of STAT3 is required for lung cancer stem cell maintenance and tumour growth. *Commun Biol* 2024;**7**:593.
39. Wohlfromm F, Ivanisenko NV, Pietkiewicz S, König C, Seyrek K, Kähne T, et al. Arginine methylation of caspase-8 controls life/death decisions in extrinsic apoptotic networks. *Oncogene* 2024;**43**: 1955−71.
40. Wang Z, Li R, Hou N, Zhang J, Wang T, Fan P, et al. PRMT5 reduces immunotherapy efficacy in triple-negative breast cancer by methylating KEAP1 and inhibiting ferroptosis. *J Immunother Cancer* 2023; **11**:e006890.
41. Vander Heiden MG, Locasale JW, Swanson KD, Sharfi H, Heffron GJ, Amador-Noguez D, et al. Evidence for an alternative glycolytic pathway in rapidly proliferating cells. *Science* 2010;**329**:1492−9.
42. Wang Y, Shu H, Qu Y, Jin X, Liu J, Peng W, et al. PKM2 functions as a histidine kinase to phosphorylate PGAM1 and increase glycolysis shunts in cancer. *EMBO J* 2024;**43**:2368−96.
43. Abramson J, Adler J, Dunger J, Evans R, Green T, Pritzel A, et al. Accurate structure prediction of biomolecular interactions with AlphaFold 3. *Nature* 2024;**630**:493−500.
44. Sanati M, Figueroa-Espada CG, Han EL, Mitchell MJ, Yavari SA. Bioengineered nanomaterials for siRNA therapy of chemoresistant cancers. *ACS Nano* 2024;**18**:34425−63.
45. Yuan Y, Sun W, Xie J, Zhang Z, Luo J, Han X, et al. RNA nanotherapeutics for hepatocellular carcinoma treatment. *Theranostics* 2025;**15**:965−92.
46. Zhai J, Chen H, Wong CC, Peng Y, Gou H, Zhang J, et al. ALKBH5 drives immune suppression *via* targeting AXIN2 to promote colorectal cancer and is a target for boosting immunotherapy. *Gastroenterology* 2023;**165**:445−62.
47. Zhu J, Fu S, Zou X, Zeng H, Cui G, Peng Y, et al. PRMT5 inhibitor synergizes with chemotherapy to induce resembling mismatch repair deficiency and enhance anti-TIGIT therapy in microsatellite-stable colorectal cancer. *Adv Sci (Weinh)* 2025;**12**:e2500271.
48. Dong Z, She X, Ma J, Chen Q, Gao Y, Chen R, et al. The E3 Ligase NEDD4L prevents colorectal cancer liver metastasis *via* degradation

of PRMT5 to inhibit the AKT/mTOR signaling pathway. *Adv Sci (Weinh)* 2025;**12**:e2504704.
49. Qu S, Feng B, Xing M, Qiu Y, Ma L, Yang Z, et al. PRMT5 K240lac confers ferroptosis resistance *via* ALKBH5/SLC7A11 axis in colorectal cancer. *Oncogene* 2025;**44**:2814−30.
50. Liang Q, Gong M, Zou JH, Luo MY, Jiang LL, Wang C, et al. A phosphoglycerate mutase 1 allosteric inhibitor overcomes drug resistance to EGFR-targeted therapy *via* disrupting IL-6/JAK2/STAT3 signaling pathway in lung adenocarcinoma. *Drug Resist Updates* 2023;**68**:100957.
51. Huang K, Liang Q, Zhou Y, Jiang LL, Gu WM, Luo MY, et al. A novel allosteric inhibitor of phosphoglycerate mutase 1 suppresses growth and metastasis of non-small-cell lung cancer. *Cell Metab* 2019;**30**:1107-19.e8.
52. Wen CL, Huang K, Jiang LL, Lu XX, Dai YT, Shi MM, et al. An allosteric PGAM1 inhibitor effectively suppresses pancreatic ductal adenocarcinoma. *Proc Natl Acad Sci U S A* 2019;**116**:23264−73.
53. Sun Y, Jin X, Meng J, Guo F, Chen T, Zhao X, et al. MST2 methylation by PRMT5 inhibits Hippo signaling and promotes pancreatic cancer progression. *EMBO J* 2023;**42**:e114558.